HAL
open science

On the use of model order reduction for simulating automated fibre placement processes

Nicolas Bur, Pierre Joyot, Chady Ghnatios, Pierre Villon, Elías Cueto, Francisco Chinesta

To cite this version:

Nicolas Bur, Pierre Joyot, Chady Ghnatios, Pierre Villon, Elías Cueto, et al.. On the use of model order reduction for simulating automated fibre placement processes. Advanced Modeling and Simulation in Engineering Sciences, 2016, 3, pp.4. 10.1186/s40323-016-0056-x . hal-01533026

HAL Id: hal-01533026

https://hal.science/hal-01533026v1

Submitted on 5 Jun 2017

HAL is a multi-disciplinary open access archive for the deposit and dissemination of scientific research documents, whether they are published or not. The documents may come from teaching and research institutions in France or abroad, or from public or private research centers.

L'archive ouverte pluridisciplinaire **HAL**, est destinée au dépôt et à la diffusion de documents scientifiques de niveau recherche, publiés ou non, émanant des établissements d'enseignement et de recherche français ou étrangers, des laboratoires publics ou privés.

Distributed under a Creative Commons Attribution 4.0 International License

Bur *et al. Adv. Model. and Simul. in Eng. Sci.(2016)3:4*
DOI 10.1186/s40323-016-0056-x

Advanced Modeling and Simulation in Engineering Sciences
a SpringerOpen Journal

RESEARCH ARTICLE Open Access

On the use of model order reduction for simulating automated fibre placement processes

Nicolas Bur[1], Pierre Joyot[1], Chady Ghnatios[2,3], Pierre Villon[4], Elías Cueto[5] and Francisco Chinesta[3*]

*Correspondence: Francisco.Chinesta@ec-nantes.fr
[3]GeM Institute, École Centrale de Nantes, 1 rue de la Noë, 44321 Nantes cedex 3, France
Full list of author information is available at the end of the article

Abstract

Automated fibre placement (AFP) is an incipient manufacturing process for composite structures. Despite its conceptual simplicity it involves many complexities related to the necessity of melting the thermoplastic at the interface tape-substrate, ensuring the consolidation that needs the diffusion of molecules and control the residual stresses installation responsible of the residual deformations of the formed parts. The optimisation of the process and the determination of the process window requires a plethora of simulations because there are many parameters involved in the characterization of the material and the process. The exploration of the design space cannot be envisaged by using standard simulation techniques. In this paper we propose the off-line calculation of rich parametric solutions that can be then explored on-line in real time in order to perform inverse analysis, process optimisation or on-line simulation-based control. In particular, in the present work, and in continuity with our former works, we consider two main extra-parameters, the first related to the line acceleration and the second to the number of plies laid-up.

Keywords: Composites, Automated fibre placement, Numerical simulation, Model order reduction, PGD, Simulation based control

Background

The production of large pieces made of thermoplastic composites is a challenging issue for today's industry. Thermoplastic composites still represent a niche market because of the difficulties associated to their processing. Several reliable manufacturing processes are now available for building-up thermoplastic laminated structures. Among them, the automated fibre placement (AFP) appears to be an appealing process. In this process a tape is placed and progressively welded on the substrate consisting in the tapes previously placed. By placing additional layers in different directions, a part with desired properties and geometry can be produced. However, the welding of two thermoplastic layers requires specific physical conditions: a permanent contact, also called intimate contact, and a temperature that has to be high enough during a large enough time interval to ensure the diffusion of macromolecules, without significant material degradation [17]. Due to the low thermal conductivity of thermoplastics, a high temperature at the interface can be reached

© 2016 Bur et al. This article is distributed under the terms of the Creative Commons Attribution 4.0 International License (http://creativecommons.org/licenses/by/4.0/), which permits unrestricted use, distribution, and reproduction in any medium, provided you give appropriate credit to the original author(s) and the source, provide a link to the Creative Commons license, and indicate if changes were made.

with a local heating. AFP uses a heat source (e.g. laser) and a cylindrical consolidation roller to ensure both conditions required for the proper welding, as depicted on Fig. 1.

The numerical simulation of such a process is the subject on an intensive research work. Indeed, because of the successive heating and cooling of the structure during the addition of new tapes, residual stresses appear in the formed part. The evaluation of these residual stresses is crucial because they have a significant impact on both the mechanical properties and the geometry of the manufactured plate or shell due to the spring-back. In order to evaluate and control the evolution of such residual stresses an accurate evaluation of the thermal history is required.

Several models were proposed since the early 90's. We can mention in particular the numerical analysis made by Sonnez et al. [19] and the work by Pitchumani et al. [15] interested in the study of interfacial bonding. In the latter, the domain considered was only 2d and strong assumptions were introduced in the thermal model, in particular concerning the boundary conditions. Moreover, in order to simplify the geometry of the domain, an incoming tow was assumed instantaneously laid down all along the substrate, which is far from being the case in the real process. Finally, the thermal/mechanical contact was assumed to be perfect at the inter-ply interfaces, which again seems to be a crude assumption. First attempts of the modelling and simulations of this process can be found in [14,18].

In [8] we proposed some improvements to existing models. First of all, the domain was considered 3d and the material anisotropic. In order to take into account the imperfect adhesion at the inter-ply interface, thermal contact resistances were introduced. Regarding the mechanical problem, the incoming tow was progressively laid down on the substrate and was subjected to a tension force in order to reproduce the pre-tension applied in the real process. But actually, beyond the model itself, the numerical method employed for the solution of the thermal and mechanical problems associated to the AFP process was novel. That work represented a first step towards a global thermo-mechanical process modelling using robust and efficient numerical tools. The numerical strategy we proposed was based on the proper generalized decomposition (PGD) [1,2]. This method uses a separated representation of the unknown field, in that case temperature or displacements, and results in a tremendous reduction of the computational complexity of the model solution. Moreover, it entails the ability to introduce any type of parameters (geometrical, material, etc.) as extra-coordinates into the model, to obtain, by solving only once the resulting

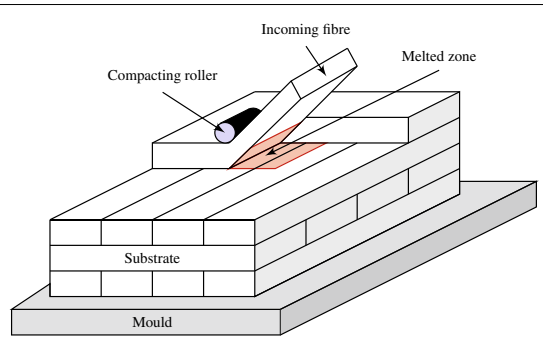

Fig. 1 Process sketch

multidimensional model, the whole envelope containing all possible solutions, a sort of computational vademecum that can be then exploited on-line even on light, deployed, computing platforms like smartphones or tablets [4,9,11,12,16].

However, in those simulations the laying velocity was considered constant. Thus, transient regimes were not taken into account, and these regimes are of special interest for controlling processes that usually involve repeated accelerations and decelerations. When accelerating, the heating power should increase to ensure melting and molecular diffusion, and when decelerating the heating power must decrease in order to prevent thermal degradation. Because the process control must operate in real time, parametric solutions should be computed off-line in order to be used on-line for process control or process optimisation Moreover, in our previous works we considered fixed the number of plies involved in the laminate, and then many parametric solutions were needed, one for each number of plies. The present work represents a step forward and considers the number of plies as a new model extra-parameter. Thermal contact resistances were successfully addressed in [8] and for the sake of simplicity, and even if they are discussed in next sections, they are not be considered in the numerical examples addressed in the last section of the present work.

The main aim of the present work is the proposal of some advanced tools for the efficient simulation of a complex composites manufacturing process, and their numerical analysis. Their consideration into an integrated simulation platform of the real industrial process is beyond the objective of the present work.

In what follows we revisit in "PGD at a glance" section the PGD discretisation technique and in "Parameters becoming coordinates" section its application for computing parametric solutions involving material parameters, initial and boundary conditions and parameters defining the domain in which the problem is defined. Modelling of the AFP manufacturing process is addressed in "Process modelling" section, with special emphasis in the consideration of the number of plies as model parameter. "From steady-state to transient parametric solutions" section focusses on transient regimes and the use of the resulting parametric solutions for process control purposes. Finally "Conclusion" section addresses few conclusions and perspectives.

PGD at a glance

Consider a problem defined in a space of dimension d for the unknown field $u(x_1, \ldots, x_d)$. Here, the coordinates x_i denote any usual coordinate (scalar or vectorial) related to physical space, time, or conformation space in microscopic descriptions [1], for example, but they could also include, as we illustrate later, model parameters such as boundary conditions or material parameters.

We seek a solution for $u(x_1, \ldots, x_d) \in \Omega_1 \times \cdots \times \Omega_d$. The PGD yields an approximate solution in the separated form

$$u(x_1, \ldots, x_d) \approx \sum_{i=1}^{N} X_i^1(x_1) \cdot \ldots \cdot X_i^d(x_d) = \sum_{i=1}^{N} \prod_{j=1}^{d} X_i^j(x_j). \tag{1}$$

The PGD approximation is thus a sum of N functional products involving each a number d of functions $X_i^j(x_j)$ that are unknown *a priori*. It is constructed by successive enrichment, whereby each functional product is determined in sequence. At a particular enrichment step $n+1$, the functions $X_i^j(x_j)$ are known for $i \leq n$ from the previous steps, and one

must compute the new product involving the d unknown functions $X^j_{n+1}(x_j)$. This is achieved by invoking the weak form of the problem under consideration. The resulting problem is non-linear, which implies that iterations are needed at each enrichment step. A low-dimensional problem can thus be defined in Ω_j for each of the d functions $X^j_{n+1}(x_j)$.

If $\mathcal{M}$ nodes are used to discretise each coordinate, the total number of PGD unknowns is $N \times \mathcal{M} \times d$ instead of the $\mathcal{M}^d$ degrees of freedom involved in standard mesh-based discretisations.

In the case of a field depending on the physical space $\mathbf{x} \in \Omega_{\mathbf{x}} \subset \mathbb{R}^3$, the time $t \in \mathcal{I}_t \subset \mathbb{R}_+$ and Q parameters $p^1, \ldots, p^Q$, where $p^j \in \Omega_{p^j}$, with $j = 1, \ldots, Q$, the solution is sought under the separated form

$$u(\mathbf{x}, t, p^1, \ldots, p^Q) \approx \sum_{i=1}^{N} \left(X_i(\mathbf{x}) \cdot T_i(t) \cdot \prod_{j=1}^{Q} P_i^j(p^j) \right). \tag{2}$$

As soon as this solution is available, after solving the multidimensional model within the PGD framework, we can have access to any possible solution.

PGD solution procedures have been extensively described in our former works and successfully applied in a plethora of applications. The interested reader can refer to the reviews [5–7] as well as to the primer [10] that describes the practical issues related to its computational implementation. For this reason in "Process modelling" section we will focus in some novel aspects that AFP processes involve. Among them we are considering two issues: (i) the consideration of the number of plies as a model parameter, allowing the solution of the thermal model for any number of plies; and (ii) the consideration of the heating cycle in a parametric way, leading to a transient parametric solution to be applied for control purposes.

Parameters becoming coordinates

In this section we summarize the developments described in [9] in order to illustrate how parameters of different nature become coordinates. In particular we consider three types of parameters: (i) parameters related to the model; (ii) parameters related to initial and boundary conditions; and (iii) geometrical parameters defining the space-time domain in which the model is defined.

Model parameters as extra-coordinates

We consider the following parametric heat transfer equation

$$\frac{\partial u}{\partial t} - k \cdot \Delta u - f = 0, \tag{3}$$

with homogeneous initial and boundary conditions. Here $(\mathbf{x}, t, k) \in \Omega \times \mathcal{I}_t \times \mathcal{I}_k$, with $\Omega \subset \mathbb{R}^3$, $\mathcal{I}_t \subset \mathbb{R}_+$ and $\mathcal{I}_k \subset \mathbb{R}$. The scalar conductivity k is here viewed as a new coordinate defined in the interval $\mathcal{I}_k$. Thus, instead of solving the thermal model for different discrete values of the conductivity parameter, we wish to solve only once a more general problem. For that purpose we consider the weighted residual form related to Eq. (3)

$$\int_{\Omega \times \mathcal{I}_t \times \mathcal{I}_k} u^* \cdot \left(\frac{\partial u}{\partial t} - k \cdot \Delta u - f \right) \mathrm{d}\mathbf{x} \cdot \mathrm{d}t \cdot \mathrm{d}k = 0. \tag{4}$$

The PGD solution is sought under the form

$$u(\mathbf{x}, t, k) \approx \sum_{i=1}^{N} X_i(\mathbf{x}) \cdot T_i(t) \cdot K_i(k). \tag{5}$$

At iteration $n < N$ the solution $u^n(\mathbf{x}, t, k)$ reads

$$u^n(\mathbf{x}, t, k) = \sum_{i=1}^{n} X_i(\mathbf{x}) \cdot T_i(t) \cdot K_i(k), \tag{6}$$

and the new trial function $u^{n+1}(\mathbf{x}, t, k)$ is searched according to

$$\begin{aligned} u^{n+1}(\mathbf{x}, t, k) &= \sum_{i=1}^{n+1} X_i(\mathbf{x}) \cdot T_i(t) \cdot K_i(k) \\ &= u^n(\mathbf{x}, t, k) + X_{n+1}(\mathbf{x}) \cdot T_{n+1}(t) \cdot K_{n+1}(k), \end{aligned} \tag{7}$$

with the test function $u^\star$ given by

$$\begin{aligned} u^\star(\mathbf{x}, t, k) = {} & X^\star(\mathbf{x}) \cdot T_{n+1}(t) \cdot K_{n+1}(k) + \\ & + X_{n+1}(\mathbf{x}) \cdot T^\star(t) \cdot K_{n+1}(k) + X_{n+1}(\mathbf{x}) \cdot T_{n+1}(t) \cdot K^\star(k). \end{aligned} \tag{8}$$

By introducing the trial and test functions, Eqs. (7) and (8) respectively, into the weak form, Eq. (4), and using an appropriate linearisation, functions $X_{n+1}(\mathbf{x})$, $T_{n+1}(t)$ and $K_{n+1}(k)$ are calculated. When considering the simplest linearisation strategy, the alternated direction fixed point algorithm, the following steps are repeated until reaching convergence:

1. With $T_{n+1}^{(r-1)}(t)$ and $K_{n+1}^{(r-1)}$ given at the previous iteration of the non linear solver $(r-1)$ (arbitrarily initialized at the first iteration: $T_{n+1}^{(0)}(t)$ and $K_{n+1}^{(0)}(k)$), all the integrals in $\mathcal{I}_t \times \mathcal{I}_k$ are performed, leading to a boundary value problem involving $X_{n+1}^{(r)}(\mathbf{x})$.
2. With $X_{n+1}^{(r)}(\mathbf{x})$ just calculated and $K_{n+1}^{(r-1)}$ given at the previous iteration of the non linear solver $(r-1)$, all the integrals in $\Omega \times \mathcal{I}_k$ are performed, leading to an one-dimensional initial value problem involving $T_{n+1}^{(r)}(t)$.
3. With $X_{n+1}^{(r)}(\mathbf{x})$ and $T_{n+1}^{(r)}$ just updated, all the integrals in $\Omega \times \mathcal{I}_t$ are performed, leading to an algebraic problem involving $K_{n+1}^{(r)}(k)$.
4. The convergence is checked by calculating

$$\begin{aligned} \mathcal{E}^r = {} & \|X_{n+1}^{(r)}(\mathbf{x}) - X_{n+1}^{(r-1)}(\mathbf{x})\| \\ & + \|T_{n+1}^{(r)}(t) - T_{n+1}^{(r-1)}(t)\| + \|K_{n+1}^{(r)}(k) - K_{n+1}^{(r-1)}(k)\|. \end{aligned} \tag{9}$$

When $\mathcal{E}^r$ becomes small enough the just computed functions are incorporated into the approximation of the solution:

$$\begin{cases} X_{n+1}(\mathbf{x}) = X_{n+1}^{(r)}(\mathbf{x}); \\ T_{n+1}(t) = T_{n+1}^{(r)}(t); \\ K_{n+1}(k) = K_{n+1}^{(r)}(k). \end{cases} \tag{10}$$

The convergence of the enrichment iteration is checked as soon as the non-linear iteration converges, by evaluating the norm of the just computed term $\|X_{n+1}(\mathbf{x}) \cdot T_{n+1}(t) \cdot K_{n+1}(k)\|$; the residual norm, or any appropriate error estimator based on quantities of interest [3].

Boundary and initial conditions as extra-coordinates

For the sake of simplicity we first consider the steady-state heat equation

$$\nabla \cdot (\mathbf{K} \cdot \nabla u(\mathbf{x})) + f(\mathbf{x}) = 0, \tag{11}$$

with $\mathbf{x} \in \Omega \subset \mathbb{R}^3$, subjected to the boundary conditions:

$$\begin{cases} u(\mathbf{x} \in \partial\Gamma_d) = u_g, \\ (-\mathbf{K} \cdot \nabla u)\,|_{\mathbf{x}\in\partial\Gamma_n} \cdot \mathbf{n} = \mathbf{q}_g \cdot \mathbf{n} = q_g, \end{cases} \tag{12}$$

with $\mathbf{K}$ the conductivity tensor and $\mathbf{n}$ the outwards unit vector defined in the domain boundary Γ_n , with $\partial\Omega \equiv \Gamma = \Gamma_d \cup \Gamma_n$ and $\Gamma_d \cap \Gamma_n = \emptyset$.

In what follows we address the simplest scenarios consisting in constant Neumann, Dirichlet and initial boundary conditions. More complex and general situations were addressed in [9].

Neumann boundary condition as extra-coordinate

First, imagine that we are interested in knowing the model solution for values of the heat flux $q_g \in \mathcal{I}_q = [q_g^-, q_g^+]$. We could consider the given heat flux as an extra-coordinate and then solving only once the resulting 4D heat equation for calculating the general parametric solution $u(\mathbf{x}, q)$. For this purpose the solution is sought under the separated form

$$u(\mathbf{x}, q_g) \approx \sum_{i=1}^{N} X_i(\mathbf{x}) \cdot \mathcal{Q}_i(q_g). \tag{13}$$

In order to enforce the prescribed Dirichlet boundary condition $u(\mathbf{x} \in \Gamma_d) = u_g$ the simplest procedure consists of choosing the first functional couple $X_1(\mathbf{x}) \cdot \mathcal{Q}_1(q_g)$ in order to ensure that $u^1(\mathbf{x} \in \Gamma_d, q_g) = X_1(\mathbf{x} \in \Gamma_d) \cdot \mathcal{Q}_1(q_g) = u_g$. Thus, the remaining terms of the finite sum $X_i(\mathbf{x})$, $i > 1$, will be subjected to homogeneous essential boundary conditions, i.e. $X_i(\mathbf{x} \in \Gamma_d) = 0$, $i > 1$.

In order to use the approximation (13) we start by considering the weak form related to Eq. (11), that writes: Find $u(\mathbf{x}) \in H^1(\Omega)$, verifying $u(\mathbf{x} \in \Gamma_d) = u_g$, such that

$$\int_\Omega \nabla u^* \cdot (\mathbf{K} \cdot \nabla u)\,\mathrm{d}\mathbf{x} = \int_{\Gamma_n} u^* \cdot (\mathbf{K} \cdot \nabla u) \cdot \mathbf{n}\,\mathrm{d}\mathbf{x} + \int_\Omega u^* \cdot f(\mathbf{x})\,\mathrm{d}\mathbf{x} \tag{14}$$

is verified $\forall u^* \in H^1(\Omega)$, with $u^*(\mathbf{x} \in \Gamma_d) = 0$.

By introducing the Neumann condition (12) into (14) it results

$$\int_\Omega \nabla u^* \cdot (\mathbf{K} \cdot \nabla u)\,\mathrm{d}\mathbf{x} = -\int_{\Gamma_n} u^* \cdot q_g\,\mathrm{d}\mathbf{x} + \int_\Omega u^* \cdot f(\mathbf{x})\,\mathrm{d}\mathbf{x}. \tag{15}$$

For using the approximation (13) we must consider the extended-weak form defined in the domain $\Omega \times \mathcal{I}_q$

$$\begin{aligned} \int_{\Omega\times\mathcal{I}_q} \nabla u^* \cdot (\mathbf{K} \cdot \nabla u)\,\mathrm{d}\mathbf{x} \cdot \mathrm{d}q_g = &-\int_{\Gamma_n\times\mathcal{I}_q} u^* \cdot q_g\,\mathrm{d}\mathbf{x} \cdot \mathrm{d}q_g \\ &+ \int_{\Omega\times\mathcal{I}_q} u^* \cdot f(\mathbf{x})\,\mathrm{d}\mathbf{x} \cdot \mathrm{d}q_g. \end{aligned} \tag{16}$$

By assuming at iteration $n+1$:

$$\begin{cases} u^* = X^*(\mathbf{x}) \cdot \mathcal{Q}_{n+1}(q_g) + X_{n+1}(\mathbf{x}) \cdot \mathcal{Q}^*(q_g); \\ u^{n+1}(\mathbf{x}, q_g) = \sum_{i=1}^{n} X_i(\mathbf{x}) \cdot \mathcal{Q}_i(q_g) + X_{n+1}(\mathbf{x}) \cdot \mathcal{Q}_{n+1}(q_g) \\ \qquad = u^n(\mathbf{x}, q_g) + X_{n+1}(\mathbf{x}) \cdot \mathcal{Q}_{n+1}(q_g). \end{cases} \tag{17}$$

Now the double iteration described in the previous section, one for enriching the separated representation and the second one for solving the non-linear problem arising at

each enrichment iteration, is performed in order to calculate the solution in separated representation.

Dirichlet boundary condition as extra-coordinate

In this section we consider that we are interested in considering the solution of model (11) for any value of u_g in (12) in a certain interval $\mathcal{I}_u = [u_g^-, u_g^+]$. For this purpose we consider the function $\varphi(\mathbf{x})$ continuous in $\overline{\Omega}$ such that $\Delta\varphi \in L_2(\Omega)$ and $\varphi(\mathbf{x} \in \Gamma_d) = 1$. Thus, we can define the change of variable [13]

$$u(\mathbf{x}) = v(\mathbf{x}) + u_g \cdot \varphi(\mathbf{x}), \tag{18}$$

that allows rewriting Eqs. (11) and (12) as

$$\nabla \cdot (\mathbf{K} \cdot \nabla v(\mathbf{x})) + u_g \cdot \nabla \cdot (\mathbf{K} \cdot \nabla \varphi(\mathbf{x})) + f(\mathbf{x}) = 0, \tag{19}$$

subjected to the boundary conditions

$$\begin{cases} v(\mathbf{x} \in \Gamma_d) = 0, \\ (-\mathbf{K} \cdot \nabla v)\,|_{\mathbf{x}\in\Gamma_n} \cdot \mathbf{n} = u_g \cdot (\mathbf{K} \cdot \nabla \varphi)\,|_{\mathbf{x}\in\Gamma_n} \cdot \mathbf{n} + q_g. \end{cases} \tag{20}$$

This results in the weak form

$$\begin{aligned} \int_\Omega \nabla v^* \cdot (\mathbf{K} \cdot \nabla v)\,\mathrm{d}\mathbf{x} &= -\int_\Omega \nabla v^* \cdot u_g \cdot (\mathbf{K} \cdot \nabla \varphi)\,\mathrm{d}\mathbf{x} \\ &+ \int_\Omega v^* \cdot f(\mathbf{x})\,\mathrm{d}\mathbf{x} - \int_{\Gamma_n} v^* \cdot q_g\,\mathrm{d}\mathbf{x} - \int_{\Gamma_n} v^* \cdot u_g \cdot (\mathbf{K} \cdot \nabla \varphi) \cdot \mathbf{n}\,\mathrm{d}\mathbf{x}. \end{aligned} \tag{21}$$

We can now introduce u_g as extra-coordinate, searching the solution under the separated form

$$v(\mathbf{x}, u_g) \approx \sum_{i=1}^{N} X_i(\mathbf{x}) \cdot \mathcal{U}_i(u_g), \tag{22}$$

that needs for the extended weak-form

$$\begin{aligned} &\int_{\Omega\times\mathcal{I}_u} \nabla v^* \cdot (\mathbf{K} \cdot \nabla v)\,\mathrm{d}\mathbf{x} \cdot \mathrm{d}u_g \\ &\quad = -\int_{\Omega\times\mathcal{I}_u} \nabla v^* \cdot u_g \cdot (\mathbf{K} \cdot \nabla \varphi)\,\mathrm{d}\mathbf{x} \cdot \mathrm{d}u_g + \int_{\Omega\times\mathcal{I}_u} v^* \cdot f(\mathbf{x})\,\mathrm{d}\mathbf{x} \cdot \mathrm{d}u_g \\ &\quad - \int_{\Gamma_n\times\mathcal{I}_u} v^* \cdot q_g\,\mathrm{d}\mathbf{x} \cdot \mathrm{d}u_g - \int_{\Gamma_n\times\mathcal{I}_u} v^* \cdot u_g \cdot (\mathbf{K} \cdot \nabla \varphi) \cdot \mathbf{n}\,\mathrm{d}\mathbf{x} \cdot \mathrm{d}u_g. \end{aligned} \tag{23}$$

on which the alternated directions fixed point algorithm applies again to calculate the parametric solution (22).

Initial conditions as extra-coordinates

We consider in this section the transient heat equation in a homogeneous and isotropic medium

$$\rho C_p \frac{\partial u}{\partial t} = k\Delta u + f, \tag{24}$$

where $t \in \mathcal{I}_t = (0, \Theta] \subset \mathbb{R}_+$, $\mathbf{x} \in \Omega \subset \mathbb{R}^3$ and $f = cte$. The initial and boundary conditions read:

$$\begin{cases} u(\mathbf{x} \in \Gamma_d) = u_g, \\ (-k\nabla u)\,|_{\mathbf{x}\in\Gamma_n} \cdot \mathbf{n} = q_g, \\ u(\mathbf{x}, t = 0) = u^0(\mathbf{x}). \end{cases} \tag{25}$$

The associated weak form reads

$$\int_{\Omega} u^* \rho C_p \frac{\partial u}{\partial t}\,\mathrm{d}\mathbf{x} + \int_{\Omega} k\nabla u^* \cdot \nabla u\,\mathrm{d}\mathbf{x} = -\int_{\Gamma_n} u^* \cdot q_g\,\mathrm{d}\mathbf{x} + \int_{\Omega} u^* \cdot f(\mathbf{x})\,\mathrm{d}\mathbf{x}, \tag{26}$$

that includes explicitly the natural (Neumann) boundary conditions. To prescribe both the initial and the essential (Dirichlet) boundary conditions we proceed to define the following functions

$$\hat{u}^0(\mathbf{x}) = \begin{cases} u^0(\mathbf{x}), & \mathbf{x} \in \Omega, \\ 0, & \mathbf{x} \in \Gamma, \end{cases} \tag{27}$$

$$\Upsilon(t) = \begin{cases} 1, & t > 0, \\ 0, & t = 0, \end{cases} \tag{28}$$

and $\varphi(\mathbf{x})$ continuous in $\overline{\Omega}$, verifying $\Delta\varphi \in L_2(\Omega)$ and the essential boundary conditions

$$\varphi(\mathbf{x} \in \Gamma_d) = u_g. \tag{29}$$

We could define the function $\Sigma(\mathbf{x}, t)$ expressed in the separated form

$$\Sigma(\mathbf{x}, t) = \hat{u}^0(\mathbf{x}) + \varphi(\mathbf{x}) \cdot \Upsilon(t) \tag{30}$$

that verifies the initial and essential boundary conditions. However, functions $\hat{u}^0$ and $\Upsilon(t)$ are not regular enough to be employed in the weak form of the problem. A direct regularisation consists in defining these functions at the nodal positions and then define interpolations with the required regularity.

By applying now the change of variable

$$u(\mathbf{x}, t) = v(\mathbf{x}, t) + \Sigma(\mathbf{x}, t) = v(\mathbf{x}, t) + \hat{u}^0(\mathbf{x}) + \varphi(\mathbf{x}) \cdot \Upsilon(t), \tag{31}$$

and approximating the initial condition as

$$\hat{u}^0(\mathbf{x}) \approx \sum_{k=1}^{S_0} U_0^k \cdot \eta_k(\mathbf{x}), \tag{32}$$

the parametric solution is assumed having the form

$$v(\mathbf{x}, U_0^1, \cdots, U_0^{S_0}) \approx \sum_{i=1}^{N} X_i(\mathbf{x}) \cdot \prod_{j=1}^{S_0} \mathcal{U}_i^j(U_0^j), \tag{33}$$

with $U_0^j \in \mathcal{I}_0^j = [(U_0^j)^-, (U_0^j)^+]$.

Parametric domains

For the sake of clarity and without loss of generality we are addressing in this section the transient one-dimensional heat equation

$$\frac{\partial u}{\partial t} = \alpha \frac{\partial^2 u}{\partial x^2} + f, \tag{34}$$

with $t \in \mathcal{I}_t = (0, \Theta] \subset \mathbb{R}$, $x \in \Omega = (0, L) \subset \mathbb{R}$, $f = cte$ and $u(x = 0, t) = u(x = L, t) = u(x, t = 0) = 0$.

The associated space-time weak form reads

$$\int_{\Omega \times \mathcal{I}_t} u^* \cdot \frac{\partial u}{\partial t}\,\mathrm{d}x\,\mathrm{d}t = -\alpha \int_{\Omega \times \mathcal{I}_t} \frac{\partial u^*}{\partial x} \cdot \frac{\partial u}{\partial x}\,\mathrm{d}x\,\mathrm{d}t + \int_{\Omega \times \mathcal{I}_t} u^* \cdot f\,\mathrm{d}x\,\mathrm{d}t. \tag{35}$$

If we are interested in computing the solution $u(x, t)$ in many domains of length $L \in [L^-, L^+]$ and for many time intervals of length $\Theta \in [\Theta^-, \Theta^+]$, more than solving the model for many possible choice in order to define a meta-model, it is preferable to compute the parametric solution $u(x, t; L, \Theta)$.

However, Eq. (35) does not involve an explicit dependence on the extra-coordinates L and Θ, both defining the domain of integration. In order to explicit this dependence, we consider the coordinate transformation

$$\begin{cases} t = \tau \cdot \Theta, \ \tau \in [0, 1], \\ x = \lambda \cdot L, \ \lambda \in [0, 1]. \end{cases} \tag{36}$$

In this case the weak form (35) now reads

$$\int_{[0,1]^2} u^* \frac{\partial u}{\partial \tau} L \, \mathrm{d}\lambda \, \mathrm{d}\tau = -\alpha \int_{[0,1]^2} \frac{\partial u^*}{\partial \lambda} \frac{\partial u}{\partial \lambda} \frac{\Theta}{L} \, \mathrm{d}\lambda \, \mathrm{d}\tau + \int_{[0,1]^2} u^* f L \Theta \, \mathrm{d}\lambda \, \mathrm{d}\tau \tag{37}$$

that allows calculating the parametric solution derived from (26) after applying the change of coordinates

$$u(\lambda, \tau, L, \Theta) \approx \sum_{i=1}^{N} \tilde{X}_i(\lambda) \cdot \tilde{T}_i(\tau) \cdot \mathcal{L}_i(L) \cdot \mathcal{T}_i(\Theta). \tag{38}$$

Process modelling

In the AFP process many parametric solutions are of interest. In [8] the authors focused on the solution of the steady-state thermal problem where the thermal contact resistances (it was proved that their consideration is a key point for modelling appropriately the thermal process), the laser power and the line velocity were considered as parameters and then included into the PGD parametric solution as extra-coordinates.

Here we extend these results by addressing two major issues: (i) the consideration of the number of plies composing the laminate as a model parameter; and (ii) the consideration of transient solutions induced by non constant laying velocities, both of major interest for controlling the process.

The numerical approaches developed in this section can be applied for any material (from the consideration of its thermal properties) and any tape dimension, with the only constraint of having a radius of curvature of the part much larger than the length of the analyzed region, such that the plane configuration analyzed remains representative. For smaller radius of curvature, it should be taken into account. Moreover, for varying tape directions thermal properties vary from one layer to other and consequently the ply orientation should be introduced as extra-parameter. This situation was successfully addressed in our former works (e.g. [4]). For the sake of clarity tape orientation is not considered in the modelling that follows.

Number of plies as parameter

First we consider the steady-state regime in the laser frame. The material domain results $\Omega = [0, L] \times [0, W] \times [0, H]$ in which we solve the heat equation

$$\rho C_p \mathbf{V} \cdot \nabla u(\mathbf{x}) = \nabla(\mathbf{K} \cdot \nabla u), \tag{39}$$

where $\mathbf{V}$ is the line velocity assumed constant ($\mathbf{V}^T = (V, 0, 0)$) and $\mathbf{K}$ the conductivity tensor. The domain thickness consists of p plies with equal thickness e_p, such that $H = p \cdot e_p$.

The boundary conditions are given by (see Fig. 2):

$$\begin{cases} u(\mathbf{x} \in \Gamma_D) = u_g, \\ -(\mathbf{K} \cdot \nabla u) \cdot \mathbf{n}\big|_{\mathbf{x} \in \Gamma_N} = q_g(\mathbf{x}) = 0, \\ -(\mathbf{K} \cdot \nabla u) \cdot \mathbf{n}\big|_{\mathbf{x} \in \Gamma_L} = q_g(\mathbf{x}) = \Phi(\mathbf{x}), \\ -(\mathbf{K} \cdot \nabla u) \cdot \mathbf{n}\big|_{\mathbf{x} \in \Gamma_R} = h(\mathbf{x})(u(\mathbf{x}) - u_{ext}), \end{cases} \tag{40}$$

where $\Gamma_D = (L, y, z)$, $\Gamma_N = \{(0, y, z) \cup (x, 0, z) \cup (x, W, z)\}$, Γ_L represents the zone in which the laser applies ($\Gamma_L = (x \in (x_r - L_\Phi, x_r + L_\Phi), y, z = H)$), and $\Phi(\mathbf{x})$ the laser heat flux. In the remaining part of the boundary convective heat exchanges occur, governed by the hydrodynamic coefficient $h(\mathbf{x})$ that takes different values on $\Gamma_M = (x, y, 0)$ where the part is in contact with the mould and on the upper surface in contact with the air $\Gamma_a = (x \in \{(0, x_r - L_\Phi) \cup (x_r + L_\Phi, L)\}, y, H)$.

Moreover, due to an imperfect consolidation at the ply interfaces $\Gamma_i = \{(x, y, e_p) \cup (x, y, 2e_p) \cup \cdots \cup (x, y, (p-1)e_p)\}$, with $p > 1$, a thermal resistance must be considered

$$-(\mathbf{K} \cdot \nabla u) \cdot \mathbf{k}\big|_{x,y,(l \cdot e_p)^-} = -(\mathbf{K} \cdot \nabla u) \cdot \mathbf{k}\big|_{x,y,(l \cdot e_p)^+}, \tag{41}$$

where

$$-(\mathbf{K} \cdot \nabla u) \cdot \mathbf{k}\big|_{x,y,(l \cdot e_p)^-} = h_i(u(x, y, (l \cdot e_p)^-) - u(x, y, (l \cdot e_p)^+)) \tag{42}$$

with $l = 1, \cdots, p-1$, p the number of plies and h_i the interface thermal resistance.

Domain transformation

When the number of plies becomes a parameter, the domain thickness H depends on the considered number of plies as depicted in Fig. 3. In order to define the problem in a reference domain we consider the coordinate transformation

$$z = \lambda \cdot p \cdot e_p, \tag{43}$$

with $\lambda \in [0, 1]$.

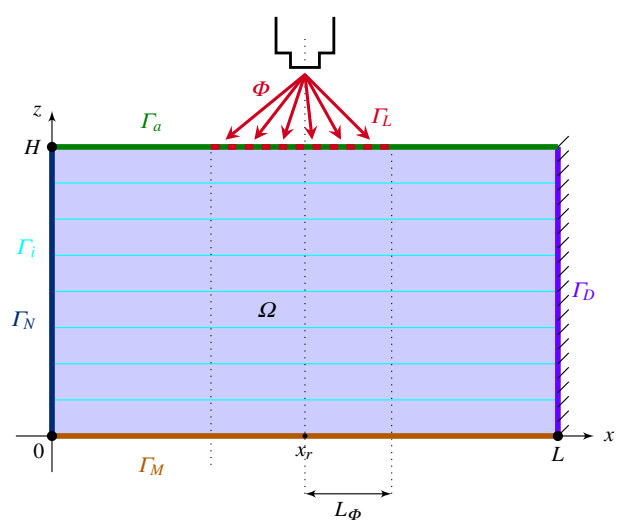

Fig. 2 Problem domain and notation

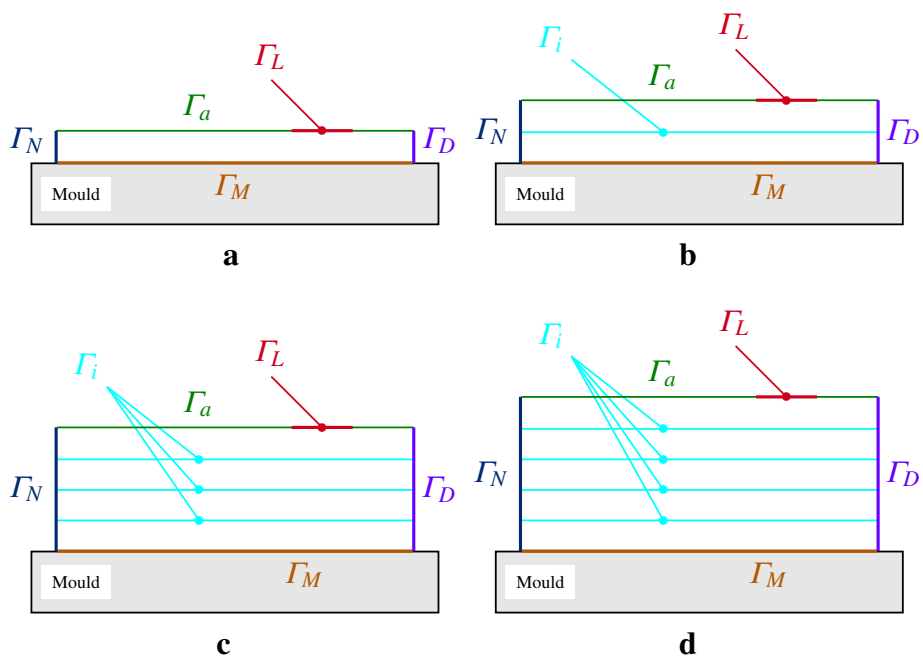

Fig. 3 Evolution of the domain with the number of plies: **a** $p = 1$; **b** $p = 2$; **c** $p = 4$ and **d** $p = 5$

The derivatives are transformed according to

$$\frac{\partial}{\partial z} = \frac{\partial}{\partial \lambda}\frac{d\lambda}{dz} = \frac{\partial}{\partial \lambda}\frac{1}{e_p p}. \tag{44}$$

Now the most natural choice for the parametric solution within the PGD framework consists of $u(x, y, \lambda, p)$ where for taking into account the discrete nature of the extra-coordinate p it suffices considering $p \in \mathcal{I}_p = [1, 2, \cdots, P_M]$, $P_M \in \mathbb{N}$. The fact of having a discrete nature is not an issue because the model does not imply derivatives with respect to the coordinate p.

Interface treatment

The fact of considering the number of plies as extra-coordinates does not represent serious difficulties if the interfaces were perfectly consolidated ensuring the temperature continuity across all them. In that case it suffices considering the separated representation

$$u(x, y, \lambda, p) \approx \sum_{i=1}^{N} X_i(x) \cdot Y_i(y) \cdot \mathcal{L}_i(\lambda) \cdot \mathcal{P}_i(p) \tag{45}$$

that injected into the weak form of Eq. (39) and proceeding as illustrated in section 3 allows calculating the parametric thermal field for any number of plies $p \in \mathcal{I}_p$.

However, when interfacial thermal resistances must be considered an important issue appears suddenly. First we must take into account the temperature discontinuity across the plies interfaces. The simplest possibility consists in duplicating the nodes at those interfaces. However the interfaces positions depend on the number of plies considered. For example when considering two plies ($p = 2$) the interface is located at $\lambda = 1/2$. When considering three plies ($p = 3$) the two interfaces are located at $\lambda = 1/3$ and $\lambda = 2/3$.

The most direct solution consists in duplicating all the nodes located at any possible interface. Thus for example if $P_M = 3$, we must take into account the interface located at $\lambda = 1/2$ for $p = 2$ and the two interfaces $\lambda = 1/3$ and $\lambda = 2/3$ associated with $p = 3$. Thus, finally the simplest solution consists in duplicating nodes located at $\lambda = 1/3$, $\lambda = 1/2$ and $\lambda = 2/3$ in order to represent any interface. However we must pay special attention when considering the interface transmission conditions, because for example for $p = 3$ we should enforce temperature discontinuity at $\lambda = 1/3$ and $\lambda = 2/3$ but perfect continuity at $\lambda = 1/2$ because when operating with $p = 3$, $\lambda = 1/2$ is not a real interface and then temperature continuity must be enforced. This situation is illustrated in Fig. 4.

In order to keep a unified description of interface conditions, needing for each p the consideration of both continuity and discontinuity transmission conditions, we propose enforcing continuity by applying the Nitsche's method. Imagine for a while that we are solving

$$-\Delta u = f, \tag{46}$$

with $u = u_0$ in $\Gamma = \partial\Omega$. The Nitsche's method consists of considering the following symmetric weak form

$$\begin{aligned}\int_\Omega \nabla u^* \cdot \nabla u \,\mathrm{d}\mathbf{x} - \int_\Gamma u^* \nabla u \cdot \mathbf{n} \,\mathrm{d}\mathbf{x} - \int_\Gamma u \nabla u^* \cdot \mathbf{n} \,\mathrm{d}\mathbf{x} + \beta \int_\Gamma u u^* \,\mathrm{d}\mathbf{x} \\ = \int_\Omega u^* f \,\mathrm{d}\mathbf{x} - \int_\Gamma u_0 \nabla u^* \cdot \mathbf{n} \,\mathrm{d}\mathbf{x} + \beta \int_\Gamma u_0 u^* \,\mathrm{d}\mathbf{x},\end{aligned} \tag{47}$$

with $u \in H^1(\Omega)$, $\forall u^* \in H^1(\Omega)$, and $\beta = \frac{1}{h} \times O(10)$ where h is the cell-size.

If now we come back to the enforcement of temperature continuity across the interface located at λ_k for a certain p for which λ_k is not a real interface (it will be for another p), the transmission condition writes from one side of the interface where the temperature is denoted by u^- assuming that $u^- = u^+$, and on the other side by enforcing $u^+ = u^-$, both written by using the Nitsche's formulation (47).

On the other hand real interfaces are easily treated because the weak forms from both sides of the interface involve the interface integrals

$$\begin{cases} -\int_{\Gamma_i} u^* (\mathbf{K} \cdot \nabla u^-) \cdot \mathbf{n} \,\mathrm{d}\mathbf{x} = \int_{\Gamma_i} u^* h_i (u^- - u^+) \,\mathrm{d}\mathbf{x}, \\ -\int_{\Gamma_i} u^* (\mathbf{K} \cdot \nabla u^+) \cdot \mathbf{n} \,\mathrm{d}\mathbf{x} = \int_{\Gamma_i} u^* h_i (u^+ - u^-) \,\mathrm{d}\mathbf{x}. \end{cases} \tag{48}$$

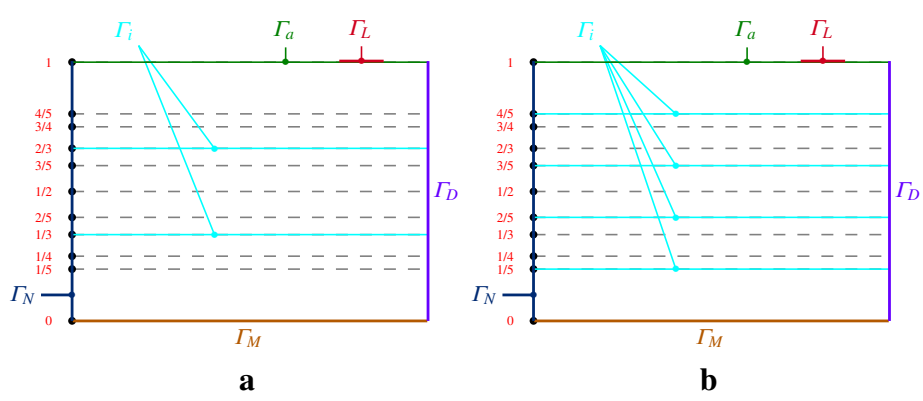

Fig. 4 Interface treatment: **a** $p = 1$ and **b** $p = 2$

Numerical results

In order to check the solution procedure we consider $L = 1$ (metric system units), $W = 0.1$, $e_p = 0.000135$, $P_M = 5$ and the thermal source applying at $x_r = 0.6$, at the tape-substrate interface $z = (p-1)e_p$, and having a distribution given by

$$\Phi(x) = qe^{-\alpha(x-\mu)^2}. \tag{49}$$

The parametric solution $u(x, y, \lambda, p)$, with $(x, y, \lambda) \in [0, L] \times [0, W] \times [0, 1]$ and $p = \{1, 2, \cdots, 5\}$, was calculated and then particularized for the different number of plies as illustrated in Fig. 5.

From steady-state to transient parametric solutions

Steady-state parametric solution

In order to control the process, other parameters should be introduced as extra-coordinates, in particular the laser power q and the line velocity V. Thus the parametric solution involves the space coordinates, the number of plies, the laser power and the line velocity, i.e. $u(x, y, \lambda, p, q, V)$.

Within the PGD framework the separated representation reads

$$u(x, y, \lambda, p, q, V) \approx \sum_{i=1}^{N} X_i(x) \cdot Y_i(y) \cdot \mathcal{L}_i(L) \cdot \mathcal{P}_i(p) \cdot \mathcal{Q}_i(q) \cdot \mathcal{V}_i(V). \tag{50}$$

Denoting by u_n^h the rank-n solution, the approximation u_{n+1}^h results from

$$\begin{aligned}&(X_{n+1}(x), Y_{n+1}(y), \mathcal{L}_{n+1}(\lambda), \mathcal{P}_{n+1}(p), \mathcal{Q}_{n+1}(q), \mathcal{V}_{n+1}(V))\\ &\quad = \underset{(X,Y,\mathcal{L},\mathcal{P},\mathcal{Q},\mathcal{V})}{\operatorname{argmin}} \|\mathbb{L}^h\left(u_n^h + X(x) \cdot Y(y) \cdot \mathcal{L}(\lambda) \cdot \mathcal{P}(p) \cdot \mathcal{Q}(q) \cdot \mathcal{V}(V)\right) - f\|,\end{aligned} \tag{51}$$

where $\mathbb{L}^h$ is the discretised operator. The enrichment is computed using a fixed point algorithm, where the minimisation of the above expression is carried out in turn on each of the 6 functions as previously described. The interested reader can refer to the primer [10] for the details on the separated representation constructor.

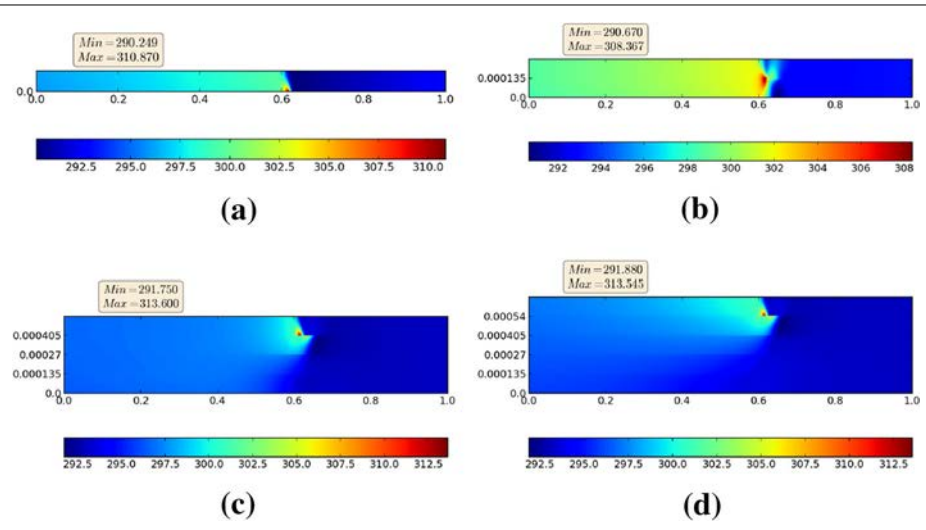

Fig. 5 Particularisation of $u(x, y, \lambda, p)$ to: **a** $p = 1$; **b** $p = 2$; **c** $p = 4$ and **d** $p = 5$

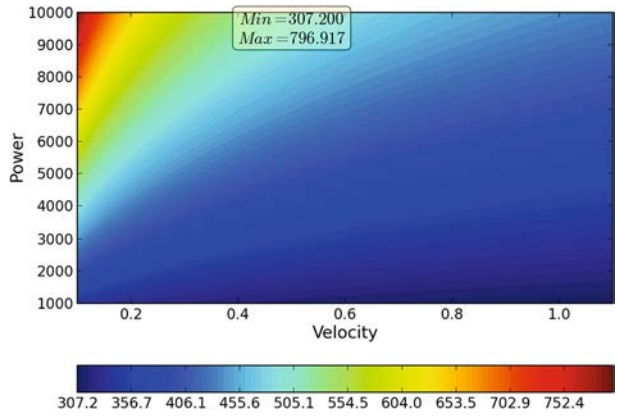

Fig. 6 Highest temperature as a function of the laser power and the line velocity when considering 8 plies: $u_8\,(q, V)$

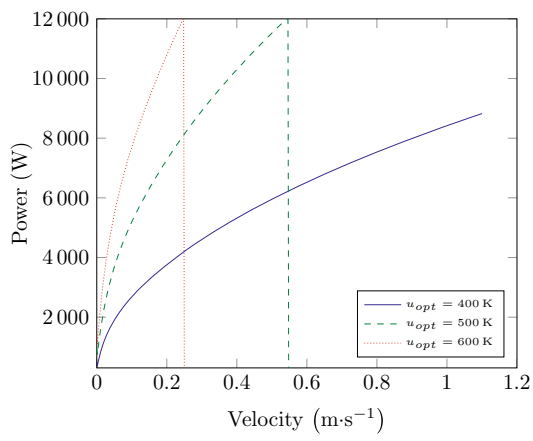

Fig. 7 Process window when considering 8 plies: $u_8\,(q, V) = u_{opt}$

Heating law determination from the steady-sate parametric solution

If one is interested by ensuring the target temperature u_{opt} at the hottest point $(x_r, W/2, (p-1)e_p)$ it suffices to extract from $u(x, y, \lambda, p, q, V)$ the following parametric solutions:

$$u_p\left(q, V; x = x_r, y = W/2, \lambda = \frac{p-1}{p}, p\right), \quad p = 2, \ldots, P_M \tag{52}$$

Fig. 6 depicts $u_8(q, V)$, that is the highest temperature as a function of the heating power and the line velocity when considering 8 plies, i.e. $p = 8$.

Now, as soon as the target temperature u_{opt} is selected, it suffices, for each number of plies, extracting from $u_p(q, V)$ the curve $u_p(p, V) = u_{opt}$. Fig. 7 depicts such a curve for three different values of the target temperature u_{opt} when considering 8 plies, associated with the parametric solution depicted in Fig. 6.

Now, we could try to use such parametric solutions for controlling transient regimes. We consider the velocity-time profile shown in Fig. 8 (blue curve) and we decided to use the parametric solution $u_8(q, V)$ for adjusting the laser power (red curve) in order to ensure a constant target temperature $u_{opt} = 400$. Fig. 8 proves that despite the fact of

using a parametric solution computed under the stationary constraint, the control seems quite good because when considering both inputs (the laser power and the line velocity) the solution of the thermal problem computed by using a space-time transient PGD (green curve) remains very close to the target temperature.

Transient parametric solution

However, a more accurate control requires the solution of the transient model and then the calculation of a parametric transient solution. In this case the time derivative of the temperature is retained in the thermal model (39) that now reads

$$\rho C_p \left(\frac{\partial u}{\partial t} + \mathbf{V} \cdot \nabla u(\mathbf{x}) \right) = \nabla(\mathbf{K} \cdot \nabla u). \tag{53}$$

Consequently the parametric solution needs considering the time and also the initial velocity and heating power as well as the accelerations of both the line velocity and the heating source, as illustrated in Fig. 9.

The thermal process is characterized by an initial interval in which the heating power and the line velocity are constants in order to reach the steady-state before enforcing the acceleration. Other options are also possible. In this case the parametric solution writes $u(x, y, \lambda, p, t, q, c, V, \Gamma)$ and within the PGD framework the separated representation writes:

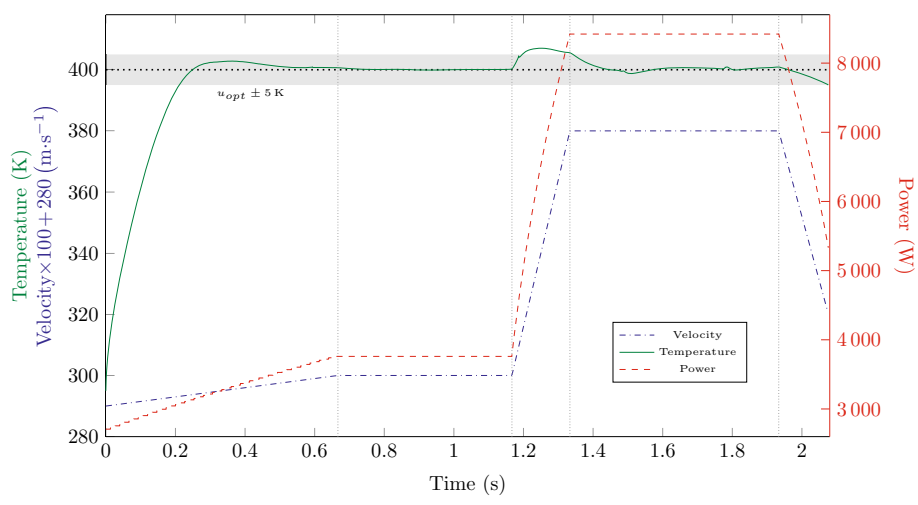

Fig. 8 Heating control from the parametric steady-state solution

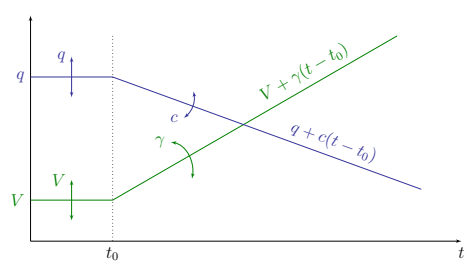

Fig. 9 modelling the transient heating: process parameters

$$u(x, y, \lambda, p, t, q, c, V, \Gamma) \approx \sum_{i=1}^{N} X_i(x) \cdot Y_i(y) \cdot \mathcal{L}_i(L) \cdot \mathcal{P}_i(p) \cdot T_i(t) \cdot \mathcal{Q}_i(q) \cdot \mathcal{C}_i(c) \cdot \mathcal{V}_i(V) \cdot \mathcal{G}_i(\Gamma) \tag{54}$$

Heating law determination from the transient parametric solution

Now, as soon as the velocity evolution is defined from Γ, we must obtain c in order to minimize the gap with respect to the target temperature. The minimisation process is illustrated in Fig. 10.

We have seen on Fig. 8 that the steady-state solution was sufficient to control the temperature, at least when the acceleration wasn't too sharp. To improve the computation of the power in this case (strong acceleration), we use the transient vademecum and the detailed method. Then, Fig. 11 proves that when making it, the procedure allows for a better fitting with respect to the target temperature (green curve). In order to compare, the dashed purple line gives the temperature using only the steady-state virtual chart (solution plotted on Fig. 8).

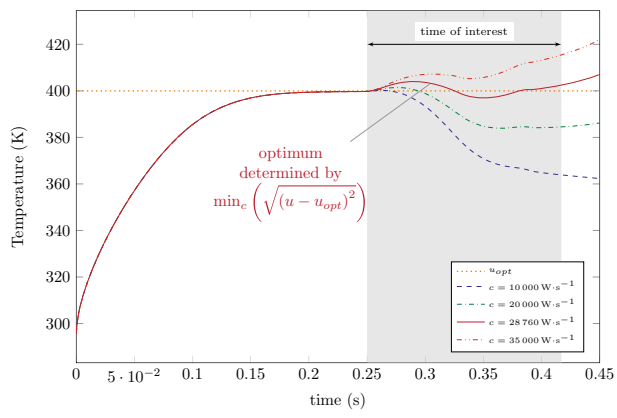

Fig. 10 Choosing the power evolution

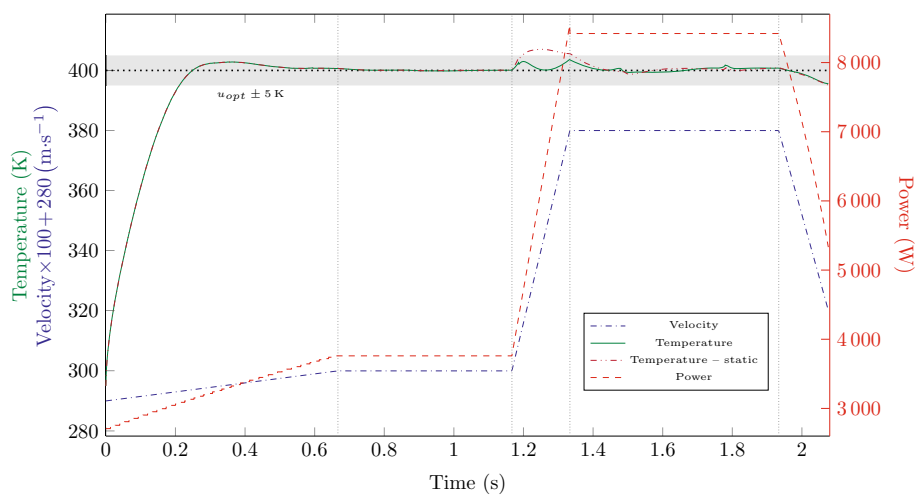

Fig. 11 Heating control from the parametric steady-state and transient solutions

Other possible computational vademecums

In order to simulate more complex scenarios involving an acceleration phase, followed by a plateau, to finish with a decelerating regime, we decided to create a parametric solution with the space coordinates, the time, three characteristic thermal resistances (one representative of the interfaces within the substrate, another representing the ply-substrate interface and lastly the one existing with the environment on the upper boundary) and the process parameters as coordinates of the system.

The process parameters concern 3 times, the plateau velocity and the plateau heating power. Thus, in the interval $[t_0 = 0, t_1]$ both velocity and laser increase linearly (with respect to time) to reach at time t_1 both target values: the plateau velocity and heating power. Then the system evolves with constant velocity and power within the interval $[t_1, t_2]$. If the length of this interval is large enough the steady-state conditions predicted by the model [8] are attained. This check served to validate transient model. Finally, within the interval $[t_2, t_3]$ both the velocity and the power decrease linearly to vanish at the terminal time t_3. The parametric solution contains in this case 12 coordinates.

Conclusion

This paper proposes an original approach to simulate AFP composites manufacturing processes. First, using a spatial transformation to match a reference domain, the number of plies composing the laminate was considered as model parameter and then as problem extra-coordinate within the PGD framework. Different parametric solutions (computational vademecums) were defined by incorporating model parameters, boundary conditions and geometrical parameters. These parametric solutions were then used in order to define the heating laws in a very simple and efficient manner. The online use of all these offline pre-computed solutions allows for real time simulation, optimization and simulation based control of heating in AFP processes. Even if the offline calculations could be expensive from the computational point of view, they are performed offline and only once. Then, further online calculation are accomplished under the real-time constraint, opening a plethora of unimaginable and appealing possibilities.

Author details
[1]ESTIA-Recherche, Technopôle Izarbel, 64210 Bidart, France, [2]Notre Dame University Louaize, P.O. Box 72, Zouk Mikael, Zouk Mosbeh, Lebanon, [3]GeM Institute, École Centrale de Nantes, 1 rue de la Noë, 44321 Nantes cedex 3, France , [4]Département Génie des systèmes mécaniques, Centre de recherches de Royallieu, Université de Technologie de Compiègne, CS 60319, 60203 Compiègne cedex, France, [5]Aragon Institute of Engineering Research, Universidad de Zaragoza, Maria de Luna s/n, 50018 Zaragoza, Spain.

Acknowledgements
This research is part of the Impala project, which is a FUI 11 project, funded by OSEO, Conseil régional d'Aquitaine and Conseil général des Pyrénées Atlantiques. Francisco Chinesta thanks the support of the *Institute Universitaire de France – IUF* – and the financial support of ESI group within the ESI-ECN Chair. Elías Cueto acknowledges the financial support of the Spanish Ministry of Economy and Competitiveness through grants number CICYT-DPI2011-27778-C02-01/02 and DPI2014-51844-C2-1-R.

Received: 14 August 2015 Accepted: 28 January 2016
Published online: 05 March 2016

References

1. Ammar A, Mokdad B, Chinesta F, Keunings R. A new family of solvers for some classes of multidimensional partial differential equations encountered in kinetic theory modelling of complex fluids. J Non Newton Fluid Mech. 2006;139:153–76.
2. Ammar A, Mokdad B, Chinesta F, Keunings R. A new family of solvers for some classes of multidimensional partial differential equations encountered in kinetic theory modelling of complex fluids. Part II: Transient simulation using space-time separated representation. J Non Newton Fluid Mech. 2007;144:98–121.

3. Ammar A, Chinesta F, Diez P, Huerta A. An error estimator for separated representations of highly multidimensional models. Comput Methods Appl Mech Eng. 2010;199:1872–80.
4. Bognet B, Leygue A, Chinesta F, Poitou A, Bordeu F. Advanced simulation of models defined in plate geometries: 3D solutions with 2D computational complexity. Comput Methods Appl Mech Eng. 2012;201:1–12.
5. Chinesta F, Ammar A, Cueto E. Recent advances and new challenges in the use of the proper generalized decomposition for solving multidimensional models. Arch Comput Methods Eng. 2010;17(4):327–50.
6. Chinesta F, Ammar A, Leygue A, Keunings R. An overview of the proper generalized decomposition with applications in computational rheology. J Non Newton Fluid Mech. 2011;166:578–92.
7. Chinesta F, Ladeveze P, Cueto E. A short review in model order reduction based on proper generalized decomposition. Arch Comput Methods Eng. 2011;18:395–404.
8. Chinesta F, Leygue A, Bognet B, Ghnatios Ch, Poulhaon F, Barasinski A, Poitou A, Chatel S, Maison-Le-Poec S. First steps towards an advanced simulation of composites manufacturing by automated tape placement. Int J Mater Form. 2014;7(1):81–92. doi:10.1007/s12289-012-1112-9.
9. Chinesta F, Leygue A, Bordeu F, Aguado JV, Cueto E, Gonzalez D, Alfaro I, Ammar A, Huerta A. Parametric PGD based computational vademecum for efficient design, optimization and control. Arch Comput Methods Eng. 2013;20(1):31–59.
10. Chinesta F, Keunings R, Leygue A. The proper generalized decomposition for advanced numerical simulations. A primer: Springerbriefs. New York: Springer; 2014.
11. Ghnatios Ch, Chinesta F, Cueto E, Leygue A, Breitkopf P, Villon P. Methodological approach to efficient modelling and optimization of thermal processes taking place in a die: Application to pultrusion. Compos Part A. 2011;42:1169–78.
12. Ghnatios Ch, Masson F, Huerta A, Cueto E, Leygue A, Chinesta F. Proper generalized decomposition based dynamic data-driven control of thermal processes. Comput Methods Appl Mech Eng. 2012;213:29–41.
13. Gonzalez D, Ammar A, Chinesta F, Cueto E. Recent advances in the use of separated representations. Int J Numer Methods Eng. 2010;81(5):637–59.
14. Lamontia M, Gruber M, Tierney J, Gillespie J, Jensen B, Cano B. Modelling the accudyne thermoplastic in situ ATP process. SAMPE Europe, March 2009, Paris.
15. Pitchumani R, Ranganathan S, Don RC, Gillespie JW. Analysis of transport phenomena governing interfacial bonding and void dynamics during thermoplastic tow-placement. Int J Heat Mass Transf. 1996;39:1883–97.
16. Pruliere E, Chinesta F, Ammar A. On the deterministic solution of multidimensional parametric models by using the proper generalized decomposition. Math Comput Simul. 2010;81:791–810.
17. Regnier G, Nicodeau C, Verdu J, Chinesta F, Cinquin J. Une approche multi-physique du soudage en continu des composites à matrice thermoplastique : vers une modélisation multi-échelle. 18e CFM, Grenoble 2007, http://documents.irevues.inist.fr/handle/2042/15971.
18. Schledjewski R, Latrille M. Processing of unidirectional fiber reinforced tapes fundamentals on the way to a process simulation tool (ProSimFRT). Compos Sci Technol. 2003;63(14):2111–8.
19. Sonmez FO, Hahn HT, Akbulut M. Analysis of process-induced residual stresses in tape placement. J Thermoplast Compos Mater. 2002;15:525–44.